AIAA 92-0178

The Dynamics and Control of Fluctuating Pressure Loads in the Reattachment Region of a Supersonic Free Shear Layer

J. Poggie, A. J. Smits,
Princeton University
Princeton, NJ

and A. Glezer
University of Arizona
Tucson, AZ

30th Aerospace Sciences Meeting & Exhibit
January 6-9, 1992 / Reno, NV

The Dynamics and Control of Fluctuating Pressure Loads in the Reattachment Region of a Supersonic Free Shear Layer

J. Poggie*, A. J. Smits†
Princeton University, Princeton, NJ
and A. Glezer‡
University of Arizona, Tucson, AZ

January 1992

Abstract

An experimental program to investigate the control of a turbulent, reattaching shear layer at Mach 2.9 is described. In preliminary experiments, schlieren photography and Rayleigh scattering were used to visualize the effects of air injection normal to the plane of the shear layer. Localized blowing was qualitatively found to increase the growth rate of the shear layer, the intensity of the turbulence, and the unsteadiness of the reattachment shock. However, uniformly distributed air injection did not appear to affect the flow strongly. These results suggest that three-dimensional disturbances are more effective for flow control than two-dimensional disturbances, and that there is a strong connection between the incoming turbulence and the shock motion in this flow.

1 Nomenclature

C_f	Skin friction coefficient
E	Anemometer output voltage
L	Intercept in hotwire calibration
M	Slope in hotwire calibration
Ma_e	Freestream Mach number
Re_θ	Momentum thickness Reynolds number
u	Local streamwise velocity
v	Local cross-stream velocity
δ	Boundary layer thickness for $0.99U_\infty$
δ_0	Boundary layer thickness at the step
ρ	Density
σ	Nondimensional shear layer growth rate: $x/(y_{0.5U_\infty} - y_{0.99U_\infty})$
Π	Turbulent boundary layer wake strength parameter
u'	$(u - \overline{u})$
$\overline{u}$	Time average of u

2 Introduction

It is well known that the combination of high temperature and large fluctuating loads greatly increases the probability of fatigue failure [1]. These factors are especially severe in the vicinity of separation and reattachment of a compressible turbulent flow. In particular, previous research (e.g. Dolling and Murphy [2]) has shown that reattachment is often accompanied by shock oscillation and intense pressure fluctuations. Further, high rates of fluctuating surface heat transfer occur near reattachment at higher Mach numbers. For example, the peak heat flux in the separated flow over a 40° compression corner at Mach 6.5 can reach a value over forty times that of an unseparated turbulent boundary layer under comparable conditions [3].

The separation/reattachment process merits detailed study due to its complexity and tendency to promote fatigue failure. Investigation of the specific problem of flow with a fixed separation point should lead to improved understanding of the more particular physics of reattachment. Such a flow offers the opportunity to investigate and eventually control the flow in the reattachment region without the complication of strong interaction between the separation and reattachment processes. These conditions are created in a model designed by Baca [4], in which the separation point of a Mach 2.9 turbulent boundary layer layer is fixed at a backward-facing step, and the shear layer reattaches on a 20° ramp (figure 1).

This paper will describe a project where air injection near the separation point in Baca's model was used to control the flow. The goals of this project are to

*Graduate Research Assistant
†Professor, Member AIAA
‡Professor, Member AIAA

enhance shear layer mixing, a topic of great interest for combustion applications, and to to help alleviate fatigue loading by reducing the intensity of pressure fluctuations at reattachment. Further, the connection between incoming turbulence and shock unsteadiness will be investigated.

2.1 Previous Research

Extensive studies have been made of the undisturbed flow field of Baca's reattaching shear layer model (Baca [4], Horstman et al. [5], Settles et al. [6], Hayakawa et al. [7], and Shen et al. [8]). The results of these studies suggest the division of the flow into four elements: the free shear layer, the recirculating cavity flow, the reattachment / shock-oscillation region, and the redeveloping boundary layer. A diagram of these flow features is given in figure 1.

Settles et al. [6] made a very complete study of the mean flow in the shear layer. They found that the velocity profiles become self-similar about 18 δ_0 downstream of separation, where δ_0 is the boundary layer thickness at the backward-facing step. The nondimensional growth rate of the shear layer (σ) was found to have a value of 28, which compares well with other experimental studies of compressible mixing layers at this Mach number. Due to the effects of compressibility on the flow turbulence, this growth rate is about one third as large as the value for a comparable subsonic shear layer (see Brown and Roshko [9], Bradshaw [10], and Settles et al. [6]).

The low-speed recirculating region in the flowfield of the model used in this study has not been surveyed because the presence of a probe in the cavity upsets the pressure balance at the separation point [4]. However, Samimy et al. [11] successfully mapped out this region with laser doppler velocimeter (LDV) measurements for a Mach 2.46 flow in a geometry similar to Baca's model. They found that the velocity of the reversed flow in the cavity can be a significant fraction of the freestream velocity (~10%). The recirculating region may be a dynamically significant flow feature because it offers a mechanism for the upstream propagation of subsonic disturbances (see Dimotakis and Brown [12], King et al. [13], and Grinstein et al. [14]).

Surface flow visualization indicates that mean reattachment occurs 67.3 $\pm$ 1.3 mm up the ramp [4]. Baca [4] suggested that certain patterns in these data reflect the presence of streamwise vortical structures, caused by a Taylor-Görtler-like instability.

Shen et al. [8] recently measured the wall pressure fluctuations in the vicinity of reattachment using high frequency miniature pressure transducers. The flow field was found to be highly unsteady with significant pressure fluctuations. Using a flow visualization method based on Rayleigh scattering, they also found shock splitting, and spanwise shock wrinkling, which may be connected with organized streamwise vorticity in the rettachment region.

A study of Baca's model using hotwire anemometry was made by Hayakawa et al. [7], focusing on the turbulence structure of the reattachment and redevelopment region. The reattachment of the shear layer was characterized by a dramatic increase in turbulence intensity $\overline{(\rho u)'^2}$ [7], followed by a gradual decrease in the redeveloping boundary layer. Similarly, Samimy et al. [11] have found an increase in turbulence intensity ($\overline{u'^2}$) and Reynolds stress ($\overline{u'v'}$) near reattachment in a similar geometry at Mach 2.46. In contrast, incompressible shear layers show a marked decrease in turbulence intensity and Reynolds stress with reattachment [15]. The drastic change in turbulence structure near reattachment has exposed many of the shortcomings of existing turbulence models [5].

Settles et al. [6] found that the redeveloping boundary layer exhibits properties far from the equilibrium case. A normal pressure gradient exists at reattachment, and weakens as the boundary layer develops. Further, a large wake component is present in the velocity profile near reattachment, due to the inflectional velocity profile of the incoming shear layer. The redeveloping velocity profile rapidly approaches the equilibrium log-wake profile, but a remarkable dip and rise behavior is evident far downstream of reattachment. Also, the intermittency of the redeveloping boundary layer is much greater than the equilibrium case.

It is interesting to compare the reattaching shear layer to the separated supersonic boundary layer induced by a ramp. Many similar features are present in the compression ramp flow studied by Selig et al. [16], for example increased turbulence intensity at reattachment followed by relaxation and redevelopment of the boundary layer, increased intermittency, and shock oscillation. Further, surface flow visualization data from the compression ramp study of Settles et al. [17] show three-dimensional structures in the reattachment region that may be evidence of streamwise vortices.

3 Experimental Procedure

3.1 Wind Tunnel Facility

The experiments described in this paper were conducted in the Princeton Gas Dynamics Laboratory 203 mm by 203 mm blowdown wind tunnel. The freestream Mach number was 2.92 $\pm$ 0.01, and the unit Reynolds number was 6.7 x 10^7 m^{-1} $\pm$ 5%. All runs were performed with a stagnation pressure of 690 kPa $\pm$ 5% and a stagnation temperature of 280 K $\pm$ 5%. Wall conditions were nearly adiabatic, and the freestream mass flux turbulence intensity was about 0.0075 [7]. More

information on the facility can be found in the report by Vas and Bogdonoff [18] and the thesis by Baca [4].

The experimental model is shown in figure 2. It consists of a wedge-shaped plate containing a cavity 25.4 mm deep, starting 229 mm downstream of the leading edge. At a distance 61.9 mm downstream of the start of the cavity, a 20° ramp, 160 mm long, lies within the cavity. When the plate is installed parallel to the freestream flow in the wind tunnel, the roof of the tunnel is 152.4 mm above the plate, and the plate spans the 203 mm width of the test section. In order to avoid interference with the side wall boundary layers, the cavity and ramp do not span the test section, but are inset by 25.4 mm on each side.

This model was designed by Baca [4] so that a fully-developed turbulent boundary layer formed on the flat plate ahead of the cavity, then separated off the backward-facing step with no change in flow direction, and finally reattached on the 20° ramp. However, the present study required optical access to the full shear layer, so that the aerodynamic fences used in Baca's experiments were removed, and the height of the cavity side walls was reduced to 15.9 mm. According to Baca [4], the removal of the aerodynamic fences does not significantly affect the flow field. Unfortunately, reducing the height of the cavity walls caused it to be impossible to exactly match the pressures in the cavity and the freestream, indicating that some three-dimensionality was present in the mean flow. Thus, a weak (Ma = 2.9 to Ma = 3.0) expansion fan existed at the lip of the cavity for the data taken in this study.

The inlet boundary condition to the cavity flow was provided by a near - equilibrium turbulent boundary layer with $Ma_e = 2.9$, $Re_\theta = 10100$, $\delta = 2.9$ mm, $C_f = 0.00144$, and $\Pi = 0.73$ at a location 25.4 mm upstream of the step [4]. The shear layer has a convective Mach number of 1.08 as calculated by the method outlined by Papamoschou and Roshko [19].

Flow control was effected by air injection through holes located near the backward - facing step. In a preliminary study, air was forced through a 3.43 mm diameter hole located 3.18 mm downstream of the step and 12.7 mm off the centerline of the model (figure 3(a)). High pressure air was provided by an adjustable pressure regulator through a 6.4 mm tube.

The model was then modified to include two spanwise rows of holes, one 12.7 mm upstream of the step, and the other 12.7 mm downstream of the step (figure 3(b)). Each row was 101.6 mm long, and consisted of 33, 1.6 mm diameter holes. In this study, the same stagnation pressure was provided to each hole, and only one row of holes was used at a time.

3.2 Flow Visualization

Two methods of flow visualization were employed in this study. First, schlieren photography was done using a Z-type schlieren system (see Baca [4]), giving an image proportional to the density gradient normal to the knife edge, averaged in the direction of the view of the camera. The mirrors in this system are 304.8 mm in diameter, and have a focal length of 2.54 m. A strobe lamp provided a flash of less than 2 μs, at a repetition rate of 30 Hz. The images were recorded by a CCD camera on 0.5 in VHS video tape. The images were digitized by an Imaging Technologies Series 151 Image Processor, but they were not enhanced or processed in any way.

A second flow visualization method was employed utilizing Rayleigh scattering of ultraviolet (UV) light (see also Smith et al. [20]). Illumination was provided by a Quantel International YG661 laser. The output of the laser was frequency-doubled to a wavelength of 266 nm, focused in one plane with a converging lens, and spread out in the perpendicular plane using a diverging lens, thus forming a trapezoidal sheet. This sheet was passed through UV-transparent quartz windows in the wind tunnel. A high-sensitivty IIT CID camera was oriented normal to this sheet, and recorded the scattered ultraviolet light via another quartz window.

The duration of the laser pulse was about 4 ns, and the thickness of the sheet of laser light was less than 0.2 mm. The UV camera had 180 lines of resolution. The data were recorded at 10 Hz, so time series information was not contained in the data.

Quantitative interpretation of the Rayleigh scattering images is hindered by the presence of ice clusters on the order of 10 nm in diameter [21]. Qualitatively, it has been observed that the ice cluster density is nearly proportional to the local air density, except when the temperature rises to a level where the ice clusters vaporize. High temperature regions therefore appear dark, as the scattering cross section of the ice clusters is much greater than that of air. However, the Rayleigh scattering technique offers a great deal of qualitative information on shock wave and shear layer structure.

3.3 Flow Surveys

An automated traversing mechanism, mounted on the tunnel ceiling, was used to make cross-stream surveys of pitot pressure, static pressure, and total temperature. A 12.7 mm maximum diameter, streamlined, hollow rod was used as a probe mount for all surveys. Pitot pressure was measured with a probe made from 0.81 mm diameter hypodermic tubing, flattened at the tip to an oval shape 0.18 mm high and 0.84 mm wide. Static pressure was measured with a conical / cylinder type probe constructed of the same tubing. It had a 15° tip,

4.5 diameters long, and two sampling holes located ten diameters downstream of the cone cylinder junction. The holes were oriented in the vertical plane to reduce sensitivity to pitch. Total temperature was measured with a chromel - alumel junction thermocouple, of 0.051 mm diameter and with a length to diameter ratio of 50. An Omega Products electronic ice point was used to as the thermocouple reference.

Constant temperature anemometry was used to measure the streamwise mass flux (ρu) according to the procedure outlined in Hayakawa et al. [7] and in Smits et al. [22]. A DISA 55M10 constant temperature anemometer was used in conjunction with a normal wire probe consisting of a 5 μm diameter tungsten wire, approximately 1 mm long, welded to stainless steel prongs. A small amount of slack was introduced into the wire to reduce the effects of strain-gaging. As noted by Hayakawa et al. [7], strain gaging can be a troublesome problem in the highly turbulent regions of the reattaching shear layer.

The hotwires used in this study were calibrated in a small Mach 3 pilot wind tunnel. The tunnel stagnation pressure was varied to attain different mass flow rates, and the data were fit to an equation of the form:

$$E^2 = L + M(\rho u)^{0.55} \quad (1)$$

where E is the anemometer output voltage, ρ is the local density, and u is the local velocity. Rong et al. [23] have determined that the calibration procedure is accurate for Mach numbers as low as 0.5 and Reynolds numbers, based on wire diameter, down to about 100.

An overheat ratio of approximately 0.8 was used in this study, and the frequency response of the hotwires as measured by the square wave test was approximately 200 kHz.

Separate mean and fluctuating signals were recorded. The anemometer output was sent both through a 10 Hz lowpass filter and recorded as the mean signal, and sent through a 10 Hz to 400 kHz bandpass filter for the fluctuating signal. The sampling rate for the fluctuating data was 1.0 MHz, and 100 352 (98k) data points were contained in one record. The data were stored and analyzed on a VAXstation 3100.

4 Results

4.1 Concentrated Blowing

As this case was intended to be a preliminary, feasibility study of blowing as a control mechanism, only visualization data were obtained. However, these data show a clear difference in the flow field when air is injected.

A supply pressure of 690 kPa $\pm$ 5% was used for the air injection in this case. Neglecting frictional losses, and assuming a Mach number of unity at the exit of the hole, the mass flux through the hole was calculated to be about 1600 kg/m^2/s and the mass flow rate to be about 0.015 kg/s. The ratio of air injection mass flux to freestream mass flux was about four, the ratio of mass flow was about 9 x 10^{-4}, and the ratio of momentum flux was about two.

Figures 5 and 6 show schlieren photographs of two views of the model. The knife edge is horizontal in these images, and the flow is from left to right. The field of view is about 87 mm by 65 mm in both sets of images, and the orientation of the views is sketched in figure 4.

Figure 5(a) shows a view of the undisturbed shear layer in the vicinity of the backward-facing step. The upper and lower edges of the developing free shear layer are clearly visible. Due to the spanwise averaging of the density gradients, the edges are almost without feature, although there is some indication of the structure of the turbulent flow. Waves are also visible emanating from the upper edge of the shear layer. There is an expansion fan centered on the edge of the fackward-facing step, indicating the mismatch between the freestream and cavity pressures. Mean flow surveys of the undisturbed case indicate that the Mach number increases from approximately 2.9 to approximately 3.0 through the expansion, resulting in a drop in static pressure of about 3 kPa.

The undisturbed case for the reattaching flow is shown in figure 6(a). The shock is evident as the dark fan-like region seen above the redeveloping boundary layer. The shock appears to be distributed in this manner for three reasons: the shock may be slightly bowed along the spanwise direction due to the absence of the aerodynamic fences, there are significant smaller scale spanwise wrinkles in the shock, and shock splitting is often present in the reattachment region (see Shen et al. [8] and the discussion following). The highly turbulent region near reattachment is visible despite the averaging across the flow caused by the schlieren technique.

Figure 5(b), shows the effect of concentrated blowing on the flow near separation. The jet is not visible in the images, primarily because of the orientation of the knife edge. Note the shock ahead of the expansion fan: this shock is produced by the jet of injected air, and it is highly three-dimensional. One surprising observation is that the shear layer deflects down (note the increased size of the expansion fan), even though mass is being added to the recirculating region, indicating that there is enhanced entrainment in the shear layer. Considerably greater activity is also seen in the recirculating flow.

The most dramatic effect of concentrated blowing is seen in the reattachment region (figure 6(b)). The increased thickness of the developing boundary layer is

obvious, as is the great distortion of the reattachment shock system. Severe curvature and strong displacement of the shock system is apparent, indicating a much higher degree of unsteadiness. Unfortunately, the dramatic nature of the increased unsteadiness cannot be conveyed through these still photographs, but is readily seen in the original videotaped images.

Rayleigh scattering images of the same flow are shown in figures 8 and 9. The flow direction in this case is from right to left, and the orientation of the views is shown in figure 7. The field of view in the images near the step is about 47 mm by 35 mm, while the field of view in the images on the ramp is about 44 mm by 33 mm. These data are interesting in that they provide a visualization of a two-dimensional, instantaneous slice of the flow field.

Figure 8 shows the top edge of the shear layer layer with and without blowing. The step is just out of the picture to the right. In constrast to the corresponding schlieren photographs, the convoluted nature of the interface is clear. The weak expansion fan is not visible, but the shock formed by the jet of injected air is visible. The increased thickness of the perturbed shear layer is apparent (the camera location was not changed for the two cases), as is the greatly increased turbulence activity near the edge of the shear layer. Compression and expansion waves appear to be closely associated with 'bulges' in the shear layer.

Figures 9 shows the reattaching flow with and without blowing. Note that the field of view is oriented along the 20° ramp in these images. Several shocks appear to exist near reattachment in both the perturbed and undisturbed cases. This feature is evident in much of the data taken. In the perturbed case, a remarkable increase in shock unsteadiness is readily apparent. The developing ramp boundary layer also appears to thicken.

4.2 Distributed Blowing

Subsequent experiments were conducted in the modified experimental model. Three cases were condsidered: the undisturbed flow, uniform blowing upstream of the step, and uniform blowing downstream of the step. It was found that the minimum stagnation pressure for blowing to have a visible effect in the schlieren photographs was 1380 kPa $\pm$ 5%, so all further experiments were conducted with this supply pressure.

The mass flux through the holes was estimated to be about 3300 kg/m^2/s and the total mass flow rate to be 0.22 kg/s. The ratio of blowing to freestream mass flux was about eight, the ratio of mass flow was about 1 x 10^{-2}, and the ratio of momentum flux was about four.

Figure 10 shows schlieren photographs of the whole model with air injection in the model cavity, while figure 11 shows the corresponding data for blowing upstream of the step. Clearly there is little difference in effect for air injection upsteam or downstream of the step. Note that the shear layer has shifted upward, in contrast to the previous results, and does not appear to thicken.

Pitot pressure, static pressure, and total temperature surveys across the shear layer were made on the centerline of the model, at the juncture of the cavity and ramp. This location was chosen because it is approximately halfway between the point where the mean velocity profiles in the undisturbed shear layer become self-similar, and the beginning of the intermittent reattachment region. In agreement with the work of Baca [4], it was found that the total temperature was constant across the shear layer within $\pm$ 2%, and that the static pressure was constant across the shear layer within $\pm$ 8%. When the mean velocity profiles were offset (by about 1 to 3 mm), the profiles collapsed onto one curve (see figure 12). Other quantities calculated from the surveys also collapse in this fashon using the same choice of offsets. The offset was probably caused by the small deflection of the shear layer as a result of blowing.

Hotwire surveys were made at the same location. As can be seen in figure 13, the hotwire mean mass flux data collapse on the same curve as the pitot data. The difference between cases in the results for root mean square fluctuating mass flux (figure 14) is within the error bands suggested by Hayakawa et al. [7] and by Smits et al. [22].

These results lead to the conclusion that the distributed blowing method merely deflects the shear layer upward by increasing the pressure in the recirculating zone. The effect of the distributed blowing on spreading rate and turbulence intensity appears to be negligible.

5 Conclusions and Future Work

Blowing can increase shear layer growth rate, turbulence intensity, and reattachment shock unsteadiness. Three-dimensional disturbances appear to have a much stronger effect on shear layer development than two-dimensional disturbances, and there seems to be a strong connection between incoming turbulence and the motion of the reattachment shock.

Future quantitative experiments will be done to confirm these conclusions. A variety of distributed blowing configurations will be studied, and compared to the uniform blowing and undisturbed cases. The goal of this work will be to find a configuration for blowing that optimizes mixing enhancement, and to search for a configuration that can reduce the intensity of pressure fluctuations at rettachment. To enable a greater control of the shear layer development, future work will also employ piezoelectric actuators as a flow control method, as

developed by Glezer for subsonic flows (e.g. see Green and Glezer [24]).

6 Acknowledgements

This work was supported by NASA Langley Grant NAG-1-1072 and AFOSR URI Grant 90-0217. Thanks go to Barry Zhang, Walter Lempert, and Phil Howard of Princeton University for assistance with the Rayleigh scattering experiments, and also to Bill Stokes, Doug Smith, and Wolfgang Konrad of the Princeton Gas Dynamics Laboratory, who have provided additional support for this project.

References

[1] Shigley, J. E., and Mitchell, L. D., *Mechanical Engineering Design*, McGraw-Hill, New York (1983).

[2] Dolling, D. S., and Murphy, M. T., *Unsteadiness of the Separation Shock Wave Structure in a Supersonic Compression Ramp Flowfield*, AIAA J., **21**, 1628 (1983).

[3] Korkegi, R. H., *Survey of Viscous Interactions Associated with High Mach Number Flight*, AIAA J., **9**, 771 (1971).

[4] Baca, B. K., *An Experimental Study of the Reattachment of a Free Shear Layer in Compressible Turbulent Flow*, M.S.E. Thesis, Princeton University, Princeton, N.J. (1981).

[5] Horstman, C.C., Settles, G. S., Williams, D. R., and Bogdonoff, S. M., *A Reattaching Free Shear Layer in Compressible Turbulent Flow*, AIAA J., **20**, 79 (1982).

[6] Settles, G. S., Baca, B. K., Williams, D. R., and Bogdonoff, S. M., *Reattachment of a Compressible Turbulent Free Shear Layer*, AIAA J., **20**, 60 (1982).

[7] Hayakawa, K., Smits, A. J., and Bogdonoff, S. M., *Turbulence Measurements in a Compressible Reattaching Shear Layer*, AIAA J., **22**, 889 (1984).

[8] Shen, Z.-H., Smith, D. R., and Smits, A. J., *Wall Pressure Measurements in the Reattachment Region of a Supersonic Free Shear Layer*, AIAA paper 90-1461 (1990).

[9] Brown, G. L., and Roshko, A., *On Density Effects and Large Structure in Turbulent Mixing Layers*, J. Fluid Mech., **64**, 775 (1974).

[10] Bradshaw, P., *Compressible Turbulent Shear Layers*, Ann. Rev. Fluid Mech., **9**, 33 (1977).

[11] Samimy, M., Petrie, H. L., and Addy, A. L., *A Study of Compressible Turbulent Reattaching Free Shear Layers*, AIAA J., **24**, 261 (1986).

[12] Dimotakis, P. E., and Brown, G. L., *The Mixing Layer at High Reynolds Number: Large-Structure Dynamics and Entrainment*, J. Fluid Mech., **78**, 535 (1978).

[13] King, R. A., Creel, T. R., and Bushnell, D. M., *Experimental Study of Free-Shear Layer Transition Above a Cavity at Mach 3.5*, AIAA paper 89-1813 (1989).

[14] Grinstein, F. F., Oran, E. S., and Boris, J. P., *Pressure Field, Feedback, and Global Instabilities of Subsonic Spatially Developing Mixing Layers*, Phys. Fluids A, **3**, 2401 (1991).

[15] Bradshaw, P., and Wong, F. Y. F., *The Reattachment and Relaxation of a Turbulent Shear Layer*, J. Fluid Mech., **52**, 113 (1972).

[16] Selig, M. S., Andreopoulos, J., Muck, K. C., Dussauge, J. P., and Smits, A. J., *Turbulence Structure in a Shock Wave / Turbulent Boundary-Layer Interaction*, AIAA J., **27**, 862 (1989).

[17] Settles, G. S., Fitzpatrick, T. J., and Bogdonoff, S. M., *A Detailed Study of Attached and Separated Compression Corner Flowfields in High Reynolds Number Supersonic Flow*, AIAA paper 78-1167 (1978).

[18] Vas, I. E., and Bogdonoff, S. M., *A Preliminary Report on the Princeton University High Reynolds Number 8in x 8in Supersonic Tunnel*, Internal Memorandum No. 39, Gas Dynamics Laboratory, Princeton University, Princeton, NJ (1971).

[19] Papamoschou, D., and Roshko, A., *The Compressible Turbulent Shear Layer: An Experimental Study*, J. Fluid Mech., **197**, 453 (1988).

[20] Smith, M. W., Smits, A. J., and Miles, R. B., *Compressible Boundary Layer Density Cross Sections by U.V. Rayleigh Scattering*, Optics Letters, **14**, 916 (1989).

[21] Wegener, P. P., and Stein G. D., *Light-Scattering Experiments and Theory of Homogeneous Nucleation in Condensing Supersonic Flow*, 12th International Symposium on Combustion, 1183 (1968).

[22] Smits, A. J., Hayakawa, K., and Muck, K. C., *Constant Temperature Hot-wire Anemometry Practice in Supersonic Flows, Part 1: The Normal Wire*, Experiments in Fluids, **1**, 83 (1983).

[23] Rong, B. S., Tan, D. K. M., and Smits, A. J., *Calibration of the Constant Temperature Normal Hot-Wire Anemometer in Transonic Flow*, Report MAE-1696, Mechanical and Aerospace Engineering Department, Princeton University, Princeton, New Jersey (1985).

[24] Green, S. M., and Glezer, A., *Manipulation of a High Aspect Ratio Rectangular Air Jet by Piezoelectric Actuators*, Forty-Fourth Annual Meeting of the American Physical Society Division of Fluid Dynamics, Scottsdale, AZ (November 1991).

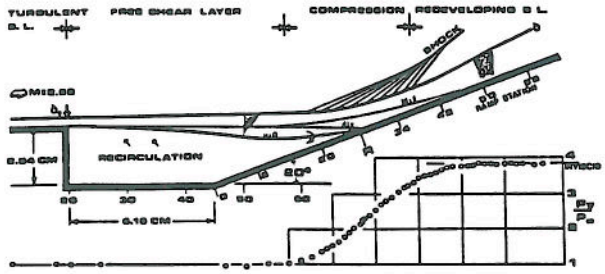

Figure 1: Diagram of Flowfield. After Baca [4].

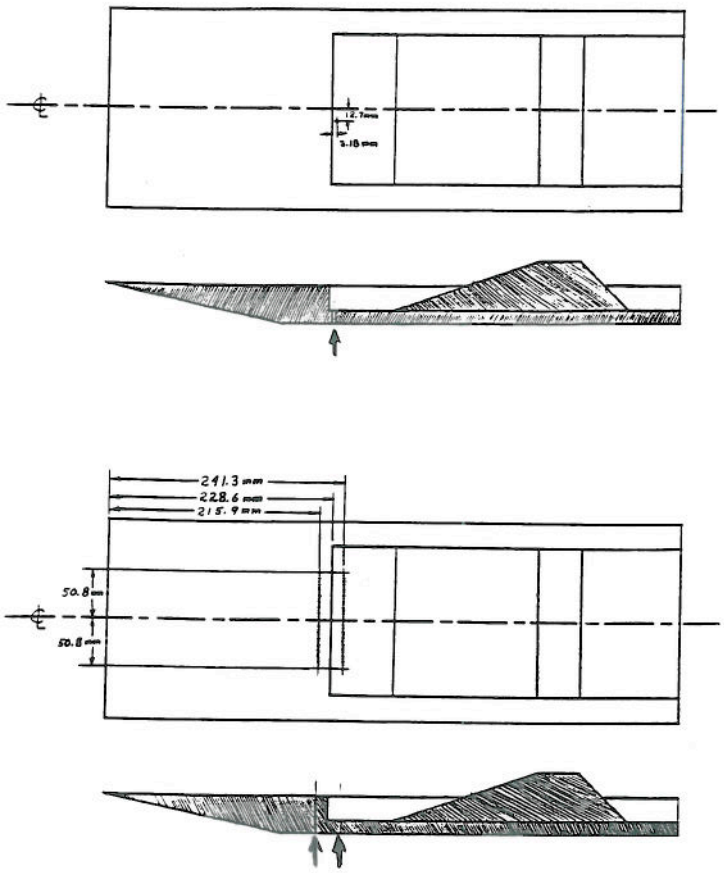

Figure 3: Modification of model for air injection. (a) concentrated blowing (b) distributed blowing.

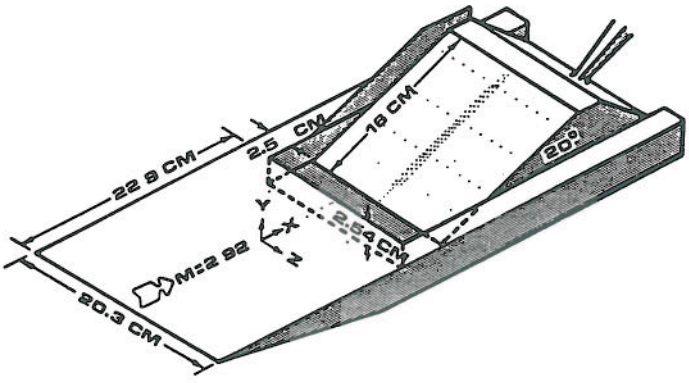

Figure 2: Experimental Model. After Baca [4].

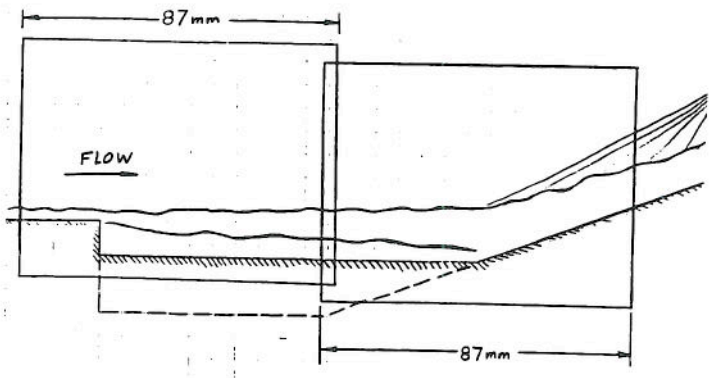

Figure 4: Field of view in schlieren photographs.

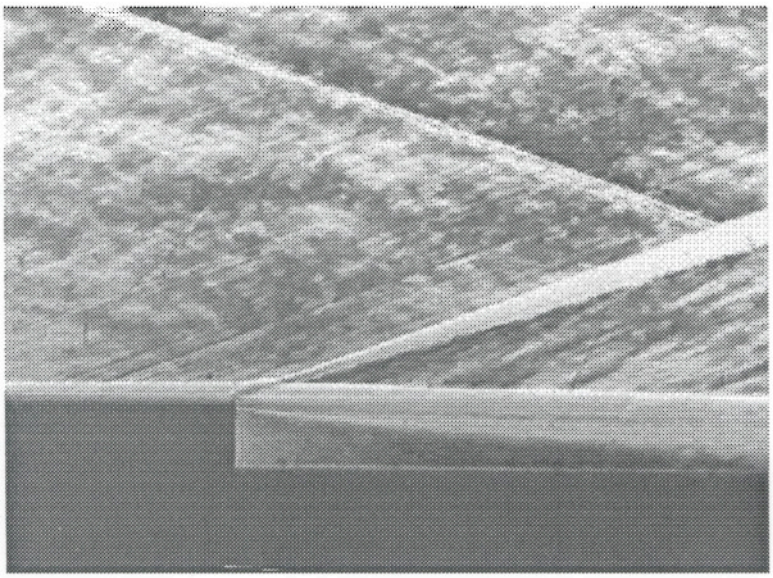

Figure 5: Schlieren photographs in the vicinity of separation. (a) undisturbed flow, (b) concentrated blowing.

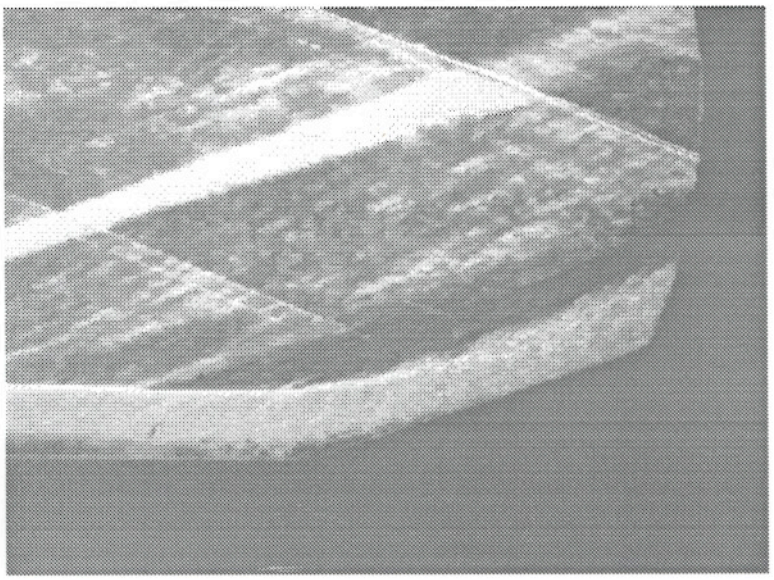

Figure 6: Schlieren photographs in the vicinity of reattachment. (a) undisturbed flow, (b) concentrated blowing.

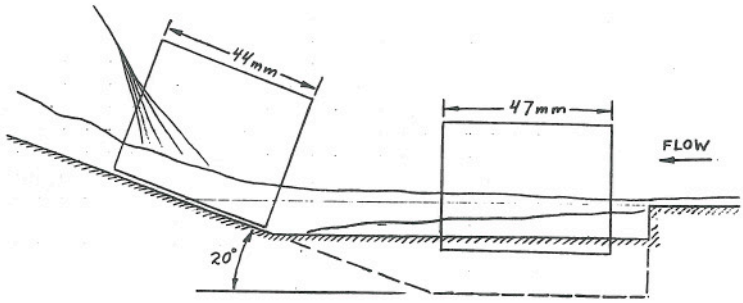

Figure 7: Field of view in Rayleigh scattering images.

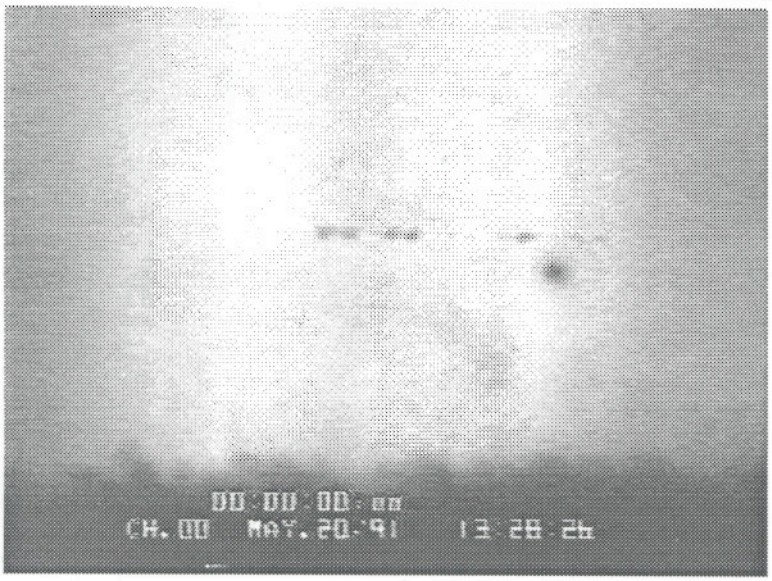

Figure 8: Rayleigh scattering images the flow in the vicinity of separation. (a) undisturbed flow, (b) concentrated blowing.

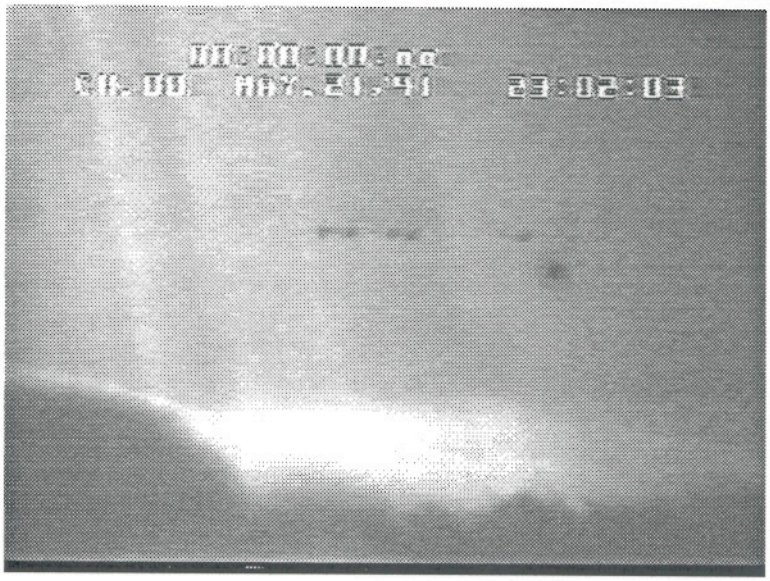

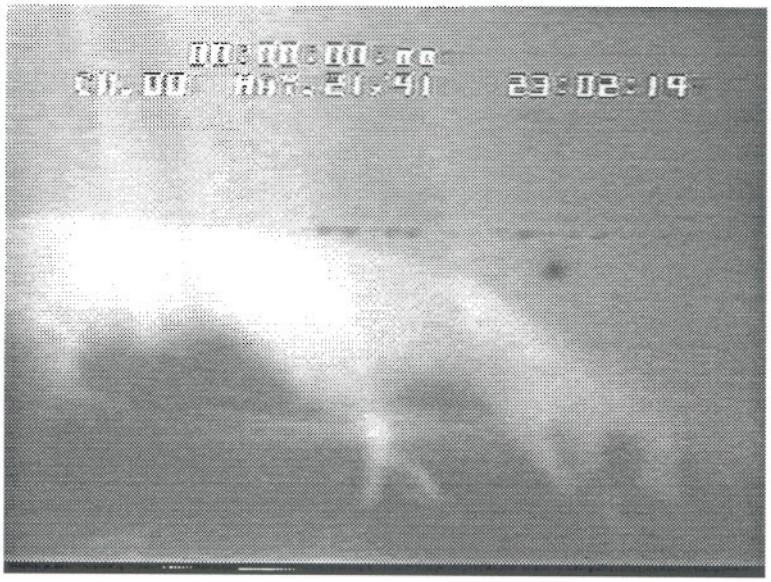

Figure 9: Rayleigh scattering images the flow in the vicinity of reattachment. Note that the horizontal axis of the images is aligned with the 20° ramp. (a) undisturbed flow, (b) concentrated blowing.

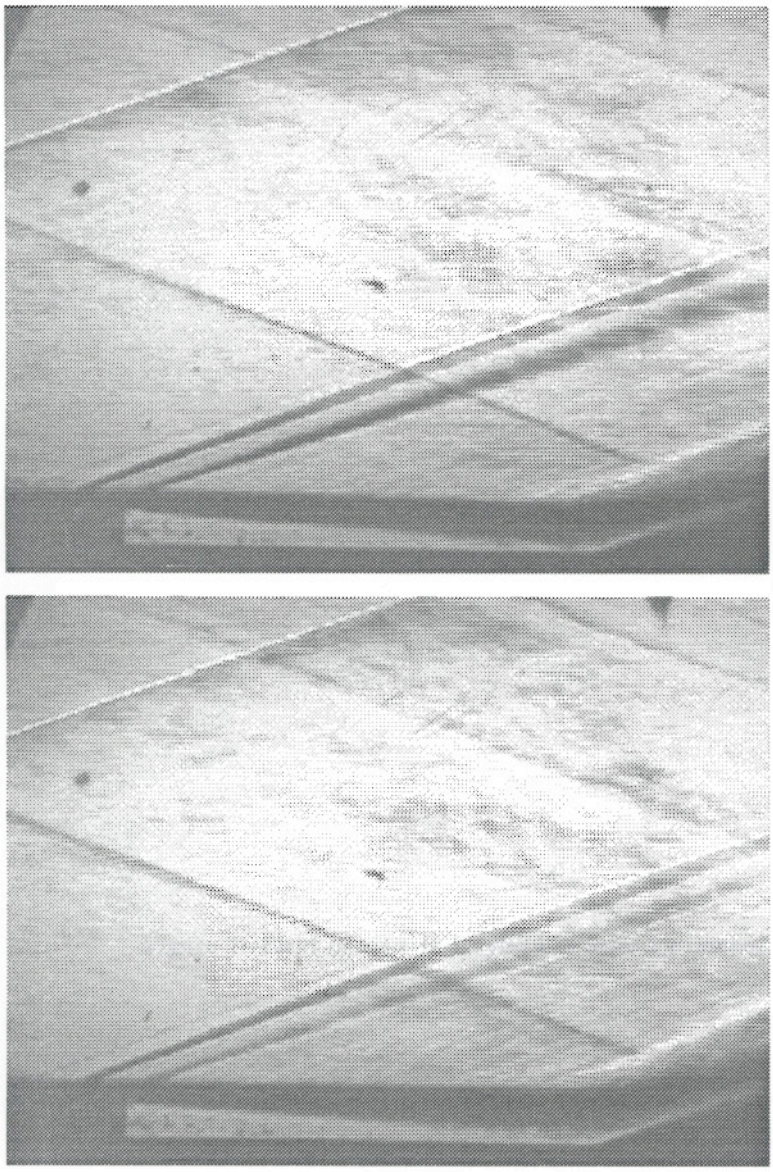

Figure 10: Schlieren photographs of distributed blowing case. (a) undisturbed flow, (b) air injection in the cavity.

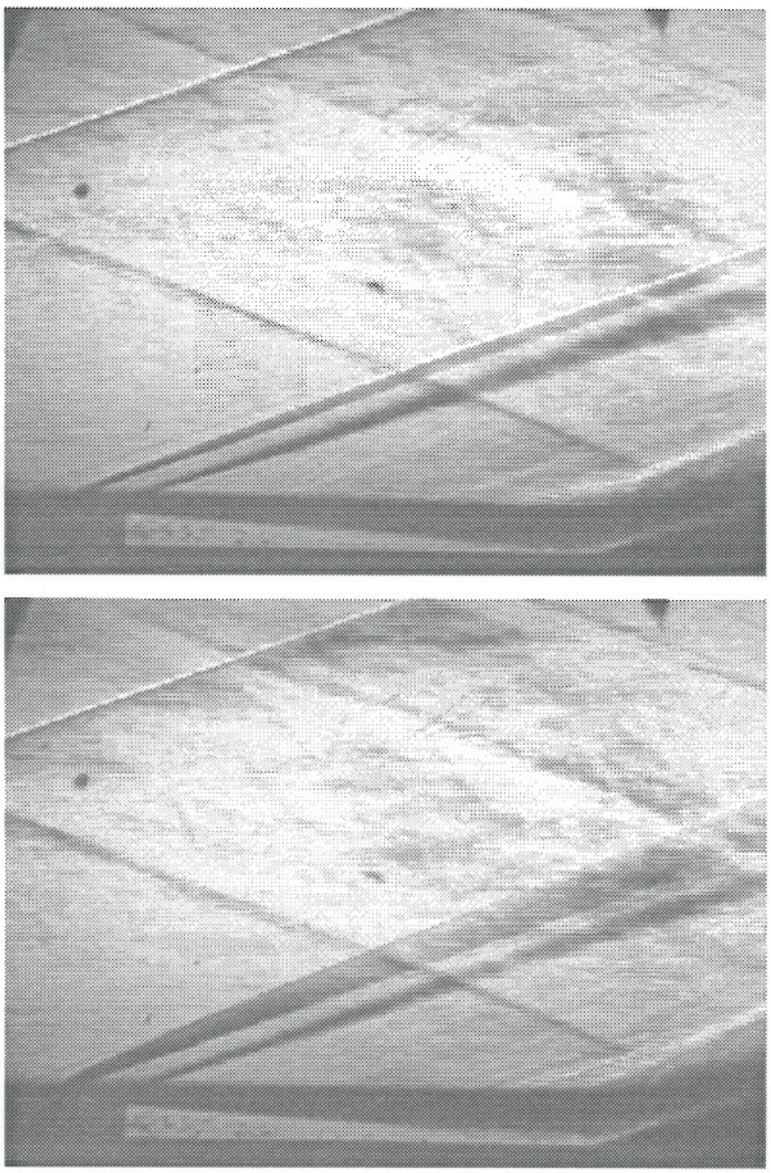

Figure 11: Schlieren photographs of distributed blowing case. (a) undisturbed flow, (b) air injection upstream of the step.

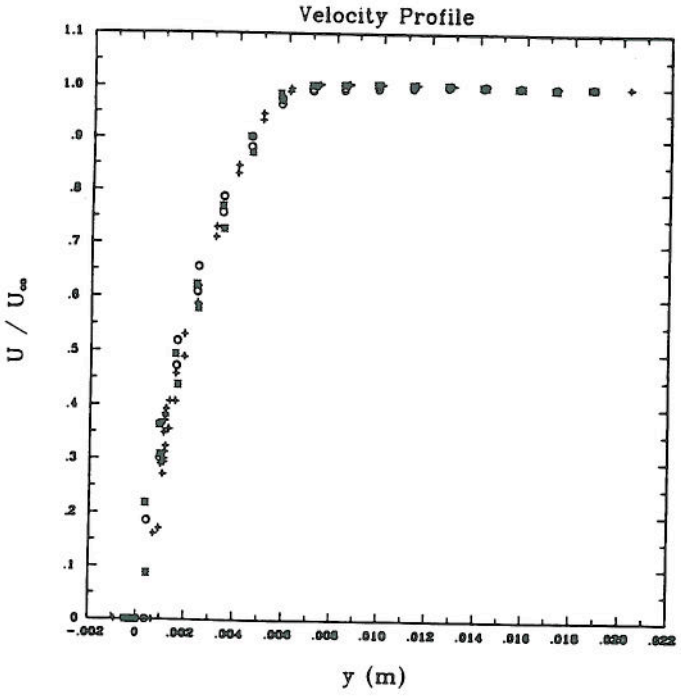

Figure 12: Velocity profiles offset to show similarity. Symbols: + - undisturbed case, * - cavity blowing, o - upstream blowing.

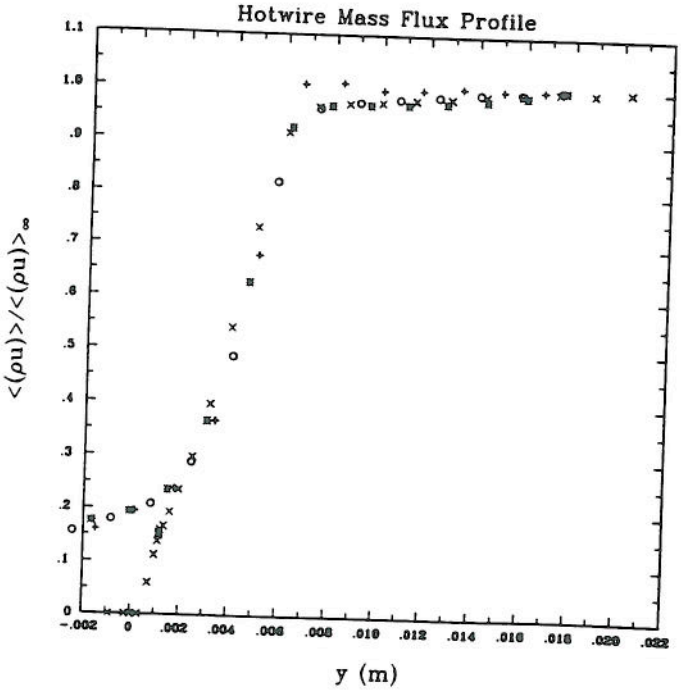

Figure 13: Mass flux profiles. Symbols: + - undisturbed case, * - cavity blowing, o - upstream blowing, × - pitot data, all cases. The calibration is not valid for $y < 0.002$ m.

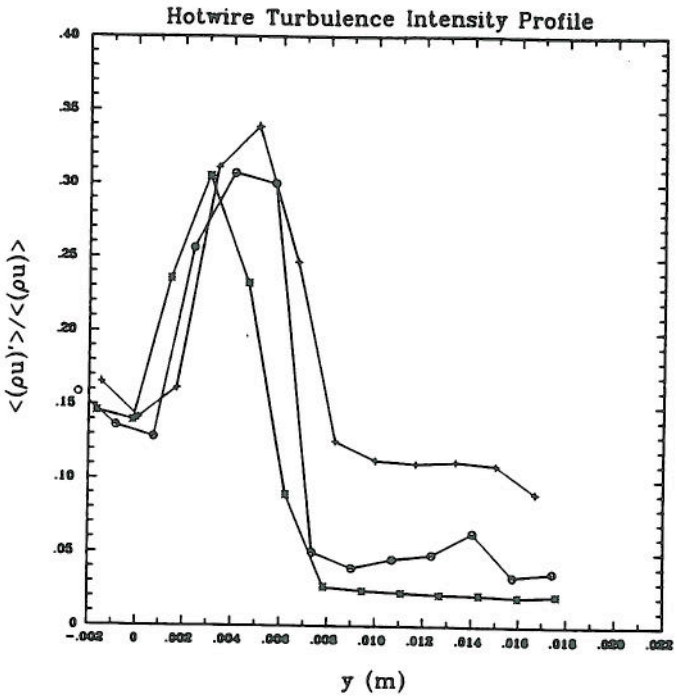

Figure 14: R.M.S. fluctuating mass flux. Symbols: + - undisturbed case, * - cavity blowing, o - upstream blowing. The calibration is not valid for $y < 0.002$ m.